Article

Direct Synthesis of In-situ Chirally Modified Palladium Nanocrystals without Capping Agents and Their Application in Heterogeneous Enantioselective Hydrogenations

Xiuyun Gao, Xueying Chen, Zhen Hua Li, and He-Yong He

ACS Catal., **Just Accepted Manuscript** • DOI: 10.1021/acscatal.9b00762 • Publication Date (Web): 28 May 2019

Direct Synthesis of In-situ Chirally Modified Palladium Nanocrystals without Capping Agents and Their Application in Heterogeneous Enantioselective Hydrogenations

Xiuyun Gao, Xueying Chen, Zhen Hua Li, and Heyong He*

Department of Chemistry and Shanghai Key Laboratory of Molecular Catalysis and Innovative Materials, Fudan University, Shanghai 200433, P. R. China

ABSTRACT: Shape-controlled metal nanocrystals possess the advantages of specific atomic arrangement on the surface and the uniform size, which can act as ideal model catalysts for heterogeneous enantioselective catalytic studies. Nevertheless, capping agents are commonly retained on the surface of the as-synthesized metal nanocrystals, which may hinder the necessary interaction between the substrate and the chiral modifiers co-adsorbed on the metal surface for chiral recognition. In this paper, we directly synthesized dendritic or cubic palladium nanocrystals in-situ modified by chiral modifiers such as cinchonidine (CD) or S-proline through a one-pot strategy by replacing the conventional capping agents with the chiral modifiers. The as-prepared CD-modified Pd nanodendrite catalyst is already to exhibit enantioselectivity in the asymmetric hydrogenation of (E)-α-phenylcinnamic acid without subsequent chiral modification

processes. The in-situ S-proline-modified Pd nanocube catalyst shows higher enantioselectivity than nanocubes synthesized with polyvinyl pyrrolidone (PVP) or cetyl trimethyl ammonium bromide (CTAB) as traditional capping agents in asymmetric hydrogenation of acetophenone. Chiral modifiers have dual functions (both shape-control agents and catalytic functional molecules), which can not only eliminate the adverse effect of traditional capping agents (such as PVP) on heterogeneous enantioselective hydrogenations, but also simplify the follow-up chiral modification step of metal catalysts, providing a simple and efficient synthetic protocol to directly prepare in-situ chirally modified metal nanocrystal catalysts.

Key words: enantioselective hydrogenation, chiral modification, palladium nanocrystals, (E)-α-phenylcinnamic acid, acetophenone

1. INTRODUCTION

The increasing demand of optically pure compounds in pharmaceutical, agrochemical and perfume industries has provided tremendous impetus for developing efficacious synthetic methods for the preparation of single-enantiomer chiral products.[1] Heterogeneous asymmetric hydrogenation of prochiral chemicals with C=C or C=O bonds is an ideal way to synthesize important chiral products due to its significant economic and ecological advantages.[2-8] Up till now, chirally modified supported metal catalysts are most extensively studied for heterogeneous enantioselective hydrogenations.[3-8] However, the difference between the energy of S and R transition states in heterogeneous asymmetric catalysis is the same as the range of various weak interactions existed on the surface of the support (e.g. hydrogen bond, physical adsorption, and van der Waals force).[9] Baiker and coworkers found that the chemoselectivity and the enantioselectivity are both greatly affected by adjusting the basicity and acidity of the support.[10]

Thus, the existence of support increases the complexity, which is disadvantageous for the in-depth study of the chiral recognition nature of heterogeneous asymmetric hydrogenation on metal surface. Therefore, it is extraordinary desirable to prepare new and effective chirally modified metal catalysts without support.

As is known, the catalytic performance of metal catalysts intensively depends on the morphology and atomic arrangement at different facets.[11-15] Thus, the preparation of metal nanocrystals exposing specific catalytically active facets has aroused great concern for decades.[13-18] However, up to the present, the application of shape-controlled metal nanocrystals is mainly focused on electrochemical tests rather than heterogeneous catalysis, especially in heterogeneous asymmetric catalysis[15]. The main reason is that the surface cleanliness of the metal nanocrystals cannot meet the requirements of heterogeneous asymmetric catalysis. As we all know, for the synthesis of shape-controllable metal nanocrystals, capping agents such as cetyl trimethyl ammonium bromide (CTAB) and polyvinyl pyrrolidone (PVP) are commonly introduced to accurately manipulate the exposed facets of the nanocrystals and inhibit aggregation.[16-19] As the capping agents have a strong adsorption on the surface of metals, they usually tend to be retained on the surface of the as-prepared metal nanocrystals and are difficult to be completely removed without changing the nanocrystal morphology, which have a major effect on the catalytic behavior of catalysts.[19-25] Our previous study demonstrated that in the enantioselective hydrogenation of acetophenone, PVP molecules residued on Pd concave-tetrahedron nanocrystals caused the enantioselectivity loss.[25] The remained PVP can interact with S-proline and hinder the necessary interaction between acetophenone and S-proline co-adsorbed on the Pd surface, inhibiting enantio-differentiation.[25] Therefore, how to prepare chirally modified metal nanocrystals without capping agents is of great significance.

Chiral modifiers, such as cinchona alkaloids and chiral amino acids, also contain specific functional groups (e.g. amino or carboxyl groups), which could bind on metal surface like conventional capping agents.[1-3, 26-27] Bönnemann and Braun applied dihydrocinchonidine to stabilize colloidal Pt nanoparticles and the nanoparticle size of Pt can be varied from 1.5 to 4 nm by changing the ratio between platinum and dihydrocinchonidine during the synthesis.[26] This system showed remarkable enantioselectivity in C=O bond hydrogenation of ethyl pyruvate.[26-27] Therefore, the chiral modifiers are possible to be used as a new category of shape-control agents in the preparation of metal nanocrystals, which can not only stabilize the metal particles but also control the morphology and exposed facets of metal nanocrystals. As both shape-control agents and chiral modification molecules, the chiral modifiers could probably not only eliminate the adverse effects of traditional capping agents on heterogeneous asymmetric hydrogenation, but also simplify the follow-up chiral modification steps.

In the present work, by replacing traditional capping agents with cinchonidine and S-proline, the two most commonly used chiral modifiers in the heterogeneous enantioselective hydrogenations, we successfully synthesized in-situ chirally modified palladium nanocrystals with different morphologies. The catalytic behaviors of the in-situ chirally modified palladium nanocrystals in the heterogeneous asymmetric hydrogenation of C=C or C=O bonds were studied. For comparison, Pd nanocrystals with similar morphology and particle size were synthesized by using conventional capping agents (PVP or CTAB) and their catalytic behaviors were also tested for evaluating the effect of chiral modifier instead of residual capping agents on the enantioselectivity. The work provides a new tactic to synthesize in-situ chirally modified metal nanocrystal catalysts with controllable shapes for heterogeneous enantioselective catalysis by eliminating the disadvantageous effect of conventional capping agents.

2. EXPERIMENTAL SECTION

2.1 Chemical and materials

Cinchonidine (CD), cinchonine (CN), S-proline, polyvinyl pyrrolidone (PVP, Mw = 55000), sodium tetrachloropalladate (Na_2PdCl_4) and (E)-α-phenylcinnamic acid (PA) were bought from Aldrich. Palladium chloride ($PdCl_2$) was obtained from J&K Scientific Ltd. Cetyl trimethyl ammonium bromide (CTAB), benzylamine (BA), ascorbic acid, hydrochloric acid, potassium bromide (KBr), 1,4-dioxane, and acetophenone were bought from Sinopharm Chemical Reagent Co., Ltd.

2.2 Catalysts synthesis

The reducing agent we used in all the synthesis is ascorbic acid. As reported in the literature[28], the reduction power of ascorbic acid is strongly related to the pH values. With the increase of pH, ascorbic acid is progressively deprotonated and the higher the pH values, the faster the reduction rate.[28] Thus, to accurately manipulate the morphology and size of Pd nanocrystals, choosing suitable Pd(II) precursors with appropriate pH values is necessary to obtain ideal reduction rates. Otherwise, Pd nanocrystals with mixed morphologies will be produced. Under acid conditions, the self-prepared H_2PdCl_4 solution with different pH values prepared by dissolving $PdCl_2$ in hydrochloric acid solution was used. Under neutral conditions, the solubility of $PdCl_2$ is low and thus commercial Na_2PdCl_4 with higher solubility is used.

Cinchonidine-modified Pd nanodendrite (Pd-dendrite-CD): 29 mg of CD was dissolved in distilled water (100 mL) at 50 °C with stirring and nitrogen protection. Then 5 mL of the aqueous solution of H_2PdCl_4 (10 mM, pH = 0.9) was added. After 3 min, ascorbic acid aqueous

solution (0.1 M, 0.8 mL, freshly prepared) was supplemented. The synthesis proceeded for 20 min at 50 °C in nitrogen atmosphere with stirring. The resulting colloids were centrifuged, washed by water once and methanol twice, then kept in 1,4-dioxane for activity test.

Cinchonine-modified Pd nanodendrite (Pd-dendrite-CN): The synthetic process is identical to the procedure described in the preparation of Pd-dendrite-CD, except using CN instead of CD.

S-Proline-modified Pd nanocube (Pd-cube-proline): 1.2 g of S-proline was added into 300 mL of deionized water under stirring and nitrogen protection at 95 °C. Then, ascorbic acid aqueous solution (0.1 M, 2.4 mL, freshly prepared) was added and stirred for 5 min, and subsequently 15 mL of H_2PdCl_4 aqueous solution (10 mM, pH = 0.9) was added. The synthesis proceeded for 20 min in nitrogen atmosphere with stirring at 95 °C. The resulting products were centrifuged, washed by water once and methanol twice, subsequently kept in methanol for activity test.

CTAB-capped Pd nanocube (Pd-cube-CTAB): The synthesis of CTAB-capped Pd nanocube was based on the previous report.[29] At 95 °C under nitrogen protection and stirring, 15 mL of H_2PdCl_4 aqueous solution (10 mM, pH = 1.7) was mixed with aqueous solution of CTAB (12.5 mM, 300 mL). 5 min later, aqueous solution of ascorbic acid (0.1 M, 2.4 mL, freshly prepared) was pipetted and the synthesis proceeded for additional 20 min. The resulting colloids were centrifuged, washed by water once and methanol twice, subsequently kept in methanol for activity test.

PVP-capped Pd nanocube (Pd-cube-PVP): The synthesis of PVP-capped Pd nanocube was based on the previous report.[30] Ascorbic acid (60 mg), KBr (600 mg), and PVP (105 mg) were dissolved in water (8.0 mL) and stirred in air at 80 °C for 10 min. Then, Na_2PdCl_4 aqueous solution (65 mM, 3.0 mL) was pipetted. The synthesis proceeded for 3 h at 80 °C. The resulting

products were centrifuged and washed by water once and methanol twice, subsequently stored with methanol for activity test.

2.3 Catalysts characterization

A JEOL 2011 transmission electron microscope (200 kV) was utilized to obtain the transmission electron microscopic (TEM) images of the samples. A FEI Tecnai G^2 F20 S-Twin field-emission transmission electron microscope (200 kV) was utilized to obtain the scanning transmission electron microscopic (STEM) images, the high-resolution TEM (HRTEM) images, the selected-area electron diffraction (SAED) patterns, and the EDX-mapping results. A Fourier transformation infrared spectrometer (FT-IR, Thermo Fisher Nicolet iS10) was used to record the spectra. The recording range is from 400 to 4000 cm^{-1} with transmission mode. The spectral resolution is 32 scans and 16 cm^{-1}. A Bruker D8 Advanced X-ray diffractometer (40 kV, 40 mA, λ = 0.15418 nm, Cu-Kα radiation) was used to record the powder X-ray diffraction (XRD) patterns.

The adsorption geometries and energies of S-proline on Pd(100) and Pd(111) surfaces were optimized by density functional theory (DFT) methods. The SIESTA package was used for calculation by utilizing the Troullier-Martins norm-conserving pseudopotentials and numerical atomic orbital basis sets[31-32]. A four-atomic-layer periodic slab with a (3×3) surface unit cell was utilized to simulate the two surfaces and the top half of atoms were allowed to relax. A vacuum layer more than 15 Å vertical to the surface was utilized to separate the slabs from their periodic images. The Monkhorst-Pack k-point sampling we utilized was (3×3×1). For the exchange-correlation functional, we applied a double-polarization basis set and the generalized gradient approximation PBE method[33]. An energy shift of 0.01 eV was applied to determine the orbital-

confining cutoff radii. 150 Rydberg was the energy cutoff set for representing the density of the real space grid. To accelerate calculations, an iterative parallel diagonalization method was applied to solve the Kohn-Sham equations and the ScaLAPACK subroutine pdsygvx was utilized employing 2D block cyclically distributed matrix[34]. We used the Broyden method to relax the geometry until all the relaxation atom forces were lower than 0.05 eV $Å^{-1}$. In all the optimizations, we consider spin polarization and fix the lattice constant of Pd to 3.95 Å[35]. The following is the formula for calculating the adsorption energies:

$$E_{ads} = E_{adsorbed} - E_{Pd} - E_{proline}$$

where $E_{adsorbed}$: optimized energy of S-proline molecule adsorbed on Pd(111) or Pd(100) surface, E_{Pd}: energy of isolated Pd surface, $E_{proline}$: energy of vacuum S-proline molecule.

2.4 Activity test

Enantioselective hydrogenation of (E)-α-phenylcinnamic acid (PA)

The reaction was conducted in a three-necked flask in 1,4-dioxane (2.5 vol% H_2O) under atmospheric pressure at ambient temperature and the H_2 flow rate was kept at 60 mL min^{-1}. 0.022 mL of BA, 4 mg of Pd-dendrite catalyst, and 76 mg of reactant PA were dispersed in 6 mL of 1,4-dioxane (2.5 vol% H_2O). BA was used as an additive in the enantioselective hydrogenation of PA, which not only enhanced the reaction rate by restructuring of the surface acid−base adducts from substrate−chiral modifier adduct to product−amine adduct, but also increased the enantioselectivity by changing the adsorption configuration of the chiral modifier on the Pd surface from N-lone pair bonded CD to π-bonded CD.[36-37] A stirring rate of 1000 rpm was kept for excluding diffusion effects. The catalytic products were identified by a high performance liquid chromatography (Agilent-1260) equipped with a chiral column (Chiralpak IG-3, 4.6 mm ×

250 mm). The retention time of the products were identified with standard chemicals. The enantioselectivity was calculated by e.e. % = |(S − R)|/(S + R) ×100.

Enantioselective hydrogenation of acetophenone

The reaction was conducted in methanol under atmospheric H_2 pressure (60 mL min^{-1}) at 273 K in a three-necked flask. Pd-cube catalyst (4 mg), S-proline (0.40 g) and acetophenone (20 μL) were dispersed in methanol (17 mL). A stirring rate of 1000 rpm was kept for excluding diffusion effects. The catalytic products were analyzed by a gas chromatography (Agilent 7820A) equipped with a chiral capillary column (CP-CHIRASIL-Dex CB, 0.25 μm × 0.32 mm × 25 m) and a flame ionization detector (FID). The products were identified with standard samples.

3. RESULTS AND DISCUSSION

3.1 Cinchonidine-modified Pd nanodendrite catalyst

3.1.1 Catalyst characterization

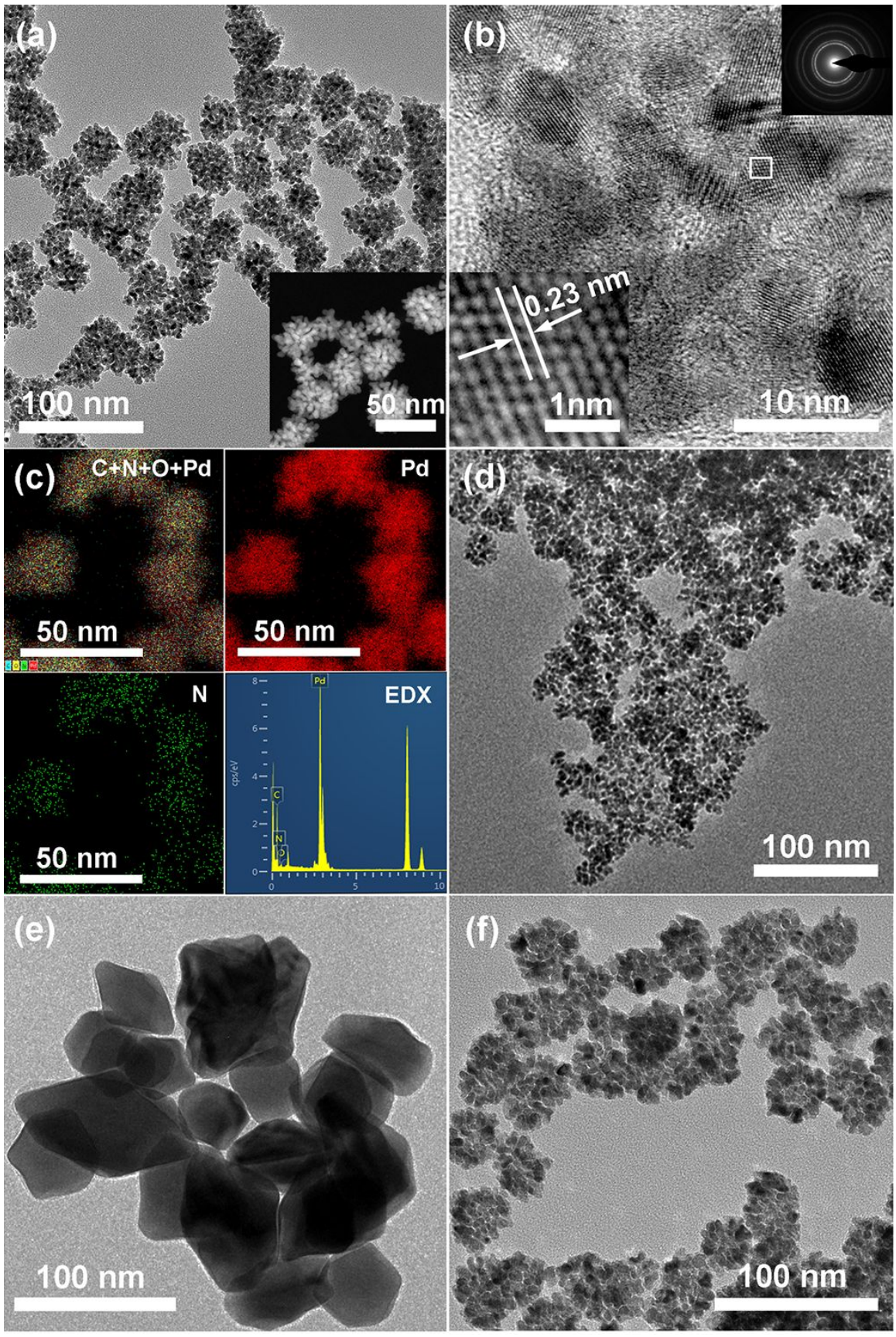
(a)
100 nm
50 nm
(b)
0.23 nm
1nm
10 nm
(c)
C+N+O+Pd
50 nm
Pd
50 nm
N
50 nm
EDX
Pd
C
N
O
cps/eV
(d)
100 nm
(e)
100 nm
(f)
100 nm

Figure 1. TEM (a), HRTEM (b), and elemental mapping results (c) of the Pd-dendrite-CD catalyst. The inset in (a) is a HAADF-STEM image of the nanodendrites. Bottom-left and top-right insets in (b) are the enlarged HRTEM image of the squared area and the corresponding SAED pattern. TEM images of (d) Pd nanocrystals prepared using 58 mg of CD, (e) Pd nanocrystals synthesized in the absence of CD, and (f) Pd-dendrite-CN catalyst.

Figure 1 presents the typical TEM, STEM, HRTEM, EDX-mapping images and SAED pattern of the Pd-dendrite-CD catalyst. As shown in Figure 1a, nanodendrites with worm-like nanostructures were produced and the average size was ~35 nm. The dendritic nature of the nanoparticles was further verified by a high-angle annular dark-field STEM image (HAADF-STEM, the inset in Figure 1a). Figure 1b shows the typical HRTEM image of a single nanodendrite. The nanodendrite was aggregated by tiny grains with the size of ~6.0 nm. SAED pattern (top-right inset in Figure 1b) reveals the polycrystalline nature of the nanodendrite. A d-spacing of 0.23 nm is observed in Figure 1b, ascribable to (111) planes of face-centered cubic (fcc) Pd[38]. Elemental analysis of the Pd-dendrite-CD sample was performed to determine the amount of CD adsorbed on the catalyst. Figure 1c presents the typical elemental mapping images of the Pd-dendrite-CD sample. The atomic ratio of N/Pd is 0.036 and the amount of CD adsorbed on Pd-dendrite-CD sample is calculated to be ca. 0.20 mg, which is ca. 5.0 wt % of the Pd catalyst. To see if it is possible to increase the amount of CD adsorbed on the catalyst, we tentatively doubled the amount of CD added in the synthetic system. Experimental results show that the resulted Pd nanocrystals no longer retain nanodendrite morphology (Figure 1d), although the N/Pd atomic ratio in this sample is slightly increased from 0.036 to 0.047.

We also synthesized palladium nanocrystals under the same synthetic conditions except for not adding CD in the synthetic system. Without the addition of CD, large Pd nanoparticles with

irregular shapes were formed and the size varied in the range of 40~100 nm (Figure 1e). This indicates that the introduction of CD is a key element for producing dendritic Pd nanocrystals. With CD, the reduction of the Pd(II) precursor leads to the production of a great number of small Pd grains and they tend to agglomerate to lower the total surface energy and form nanodendrites.[39-41]

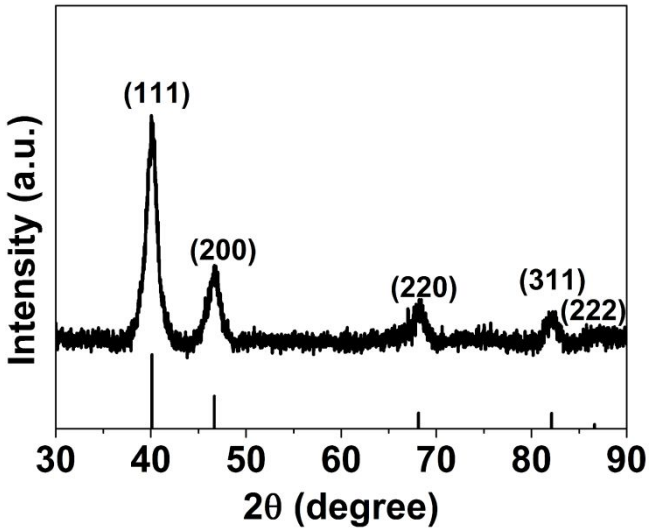

Figure 2. XRD pattern of Pd-dendrite-CD catalyst. Vertical lines represent fcc Pd (JCPDS 89-4897).

The XRD pattern of Pd-dendrite-CD catalyst (Figure 2) exhibits characteristic reflection of the Pd black (JCPDS No. 89-4897) and the lattice parameter is calculated to be 0.389 nm. The ratio of the (200) to (111) peaks in the nanodendrite sample is similar to that of Pd black sample, indicating no observed preferred orientation of the Pd-dendrite-CD catalyst.

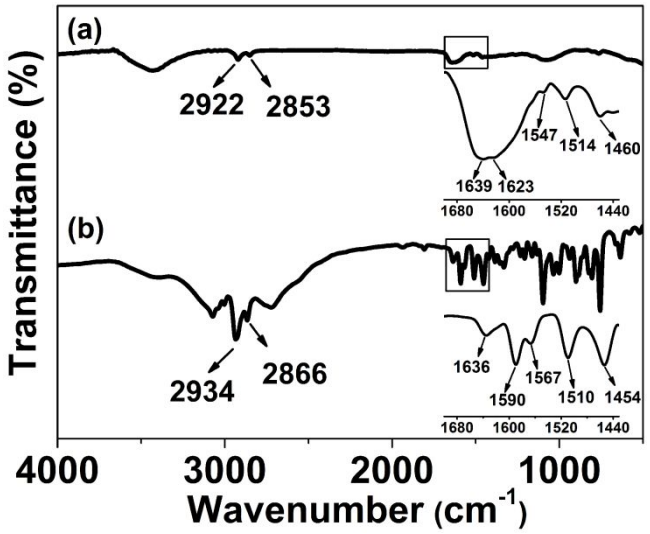

Figure 3. FT-IR spectra of Pd-dendrite-CD (a) and CD (b). Insets are enlarged spectra of the rectangular areas.

The FT-IR spectra of Pd-dendrite-CD catalyst and pure CD are shown in Figure 3. As for CD, the typical vibrational modes of vinyl ν(C=C) and the quinuclidine moieties are observed at 1636 and 1454 cm^{-1}, respectively.[42-44] Three bands corresponding to the vibrational bands of quinoline ring are observed at 1590, 1567 and 1510 cm^{-1}.[42-44] In addition, two other bands ascribable to C-H stretch modes of quinuclidine moiety from CD are also observed at 2934 and 2866 cm^{-1}.[44] As for the Pd-dendrite-CD catalyst, these vibrational bands can still be observed although there are some shifts, which is probably due to the interaction between palladium and CD.[42-44] FT-IR spectra clearly indicate that there is CD adsorbed on the as-prepared Pd nanodendrite catalyst.

3.1.2 Enantioselective hydrogenation of (E)-α-phenylcinnamic acid (PA)

The CD-modified Pd catalyst is the most widely studied heterogeneous catalyst for enantioselective hydrogenation of α,β-unsaturated carboxylic acids.[7] Therefore, we tested the

catalytic property of the as-prepared Pd-dendrite-CD catalyst by using the enantioselective hydrogenation of PA as a probe.

The yield of 2,3-diphenylpropionic acid and the enantioselectivity evolution (inset) with time on the as-synthesized Pd-dendrite-CD catalyst are plotted in Figure 4. With reaction time increasing, the yield of 2,3-diphenylpropionic acid exhibits a gradual increase. Interestingly, an average enantioselectivity of ~15% with the dominant S-enantiomer is obtained over the as-prepared Pd-dendrite-CD catalyst without the introduction of additional CD chiral modifier in the reaction mixture. This result suggests that the CD remained on the as-prepared dendritic Pd nanocrystals is already sufficient to induce chiral recognition. When we introduce another 6 mg of CD in the reaction mixture, the enantioselectivity can be further increased to 33%, although the yield of 2,3-diphenylpropionic acid decreased from 49.8% to 17.6% (Table 1, entry 2). The phenomenon of reduction in activity is similar to the literature report[7], which is probably due to that the Pd active sites are occupied by the adsorbed modifier CD[45]. After three successive runs, there was no decrease in the enantioselectivity, demonstrating the good enantioselective ability of the Pd-dendrite-CD catalyst (Table 1, entry 2-4). The decrease in the yield of 2,3-diphenylpropionic acid over the recycled Pd-dendrite-CD catalyst probably concerns with the occupation of Pd active sites by the accumulated CD adsorbed on the recycled catalysts.[7,45]

As for the heterogeneous asymmetric hydrogenation of PA, literature studies focused on supported Pd catalysts and it was found that the enantioselectivity varied significantly associated with support materials, reaction conditions and preparation methods of Pd catalysts.[36, 46-47] The highest ee reported so far is ~90% over a CD-modified Pd-TiO_2 (40 wt %) catalyst at 15 °C under optimized conditions.[47] The difficulty in achieving high ee is considered to arise from the fact that the reaction rate on unmodified Pd sites is ca. ten times faster than that on CD-modified

Pd sites.[36] Thus, the much lower ee on the Pd-dendrite-CD catalyst is probably related to the fact that only small amount of CD is adsorbed on the catalyst, as verified by the EDX-mapping analysis. The low surface coverage of adsorbed CD on the Pd-dendrite-CD catalyst is unfavorable to obtain high enantio-differentiation.

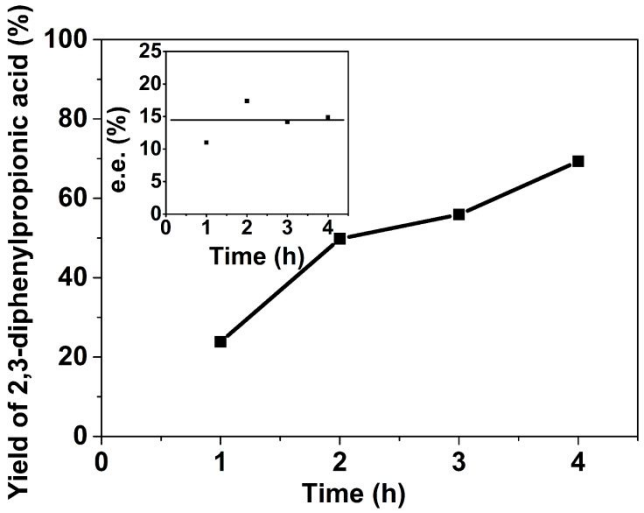

Figure 4. The yield of 2,3-diphenylpropionic acid and the enantioselectivity evolution (inset) with time on the as-synthesized Pd-dendrite-CD catalyst. Reaction conditions: ambient temperature, 76 mg reactant, 0.022 mL BA, 4 mg catalyst, 6 mL 1,4-dioxane (2.5 vol% H_2O), H_2 (60 mL min^{-1}).

Table 1. The catalytic property of as-prepared Pd-dendrite-CD and Pd-dendrite-CN samples in enantioselective hydrogenation of PA.

Entry	Catalyst	Amount of additional CD/CN added (mg)	Yield (%)	ee (%)	Dominant Enantiomer
1	Pd-dendrite-CD	0	49.8	17	S
2	Pd-dendrite-CD	6	17.6	33	S
3	Pd-dendrite-CD-2nd run	6	15.4	35	S
4	Pd-dendrite-CD-3rd run	6	12.8	34	S
5	Pd-dendrite-CN	0	48.4	9	R

Reaction conditions: ambient temperature, 76 mg reactant, 0.022 mL BA, 4 mg catalyst, 6 mL 1,4-dioxane (2.5 vol% H_2O), H_2 (60 mL min^{-1}), reaction time 2 h.

To further verify that the chirality is induced by the chiral modifier CD adsorbed on the dendritic Pd nanocrystals, we tentatively replaced CD with CN (epimer of CD) in the shape-controlled synthesis and obtained similar dendritic Pd nanocrystals (Figure 1f). The as-synthesized Pd-dendrite-CN catalyst also exhibited enantioselectivity in the enantioselective hydrogenation of PA, except that R-enantiomer was dominant (Table 1, entry 5) in contrast to the S-enantiomer dominant for the Pd-dendrite-CD catalyst. The results clearly demonstrate that CD has the dual functions of both the shape-control agent and the chiral modification molecule in our shape-controlled synthetic process.

3.2 S-Proline-modified Pd nanocube catalyst

3.2.1 Catalyst characterization

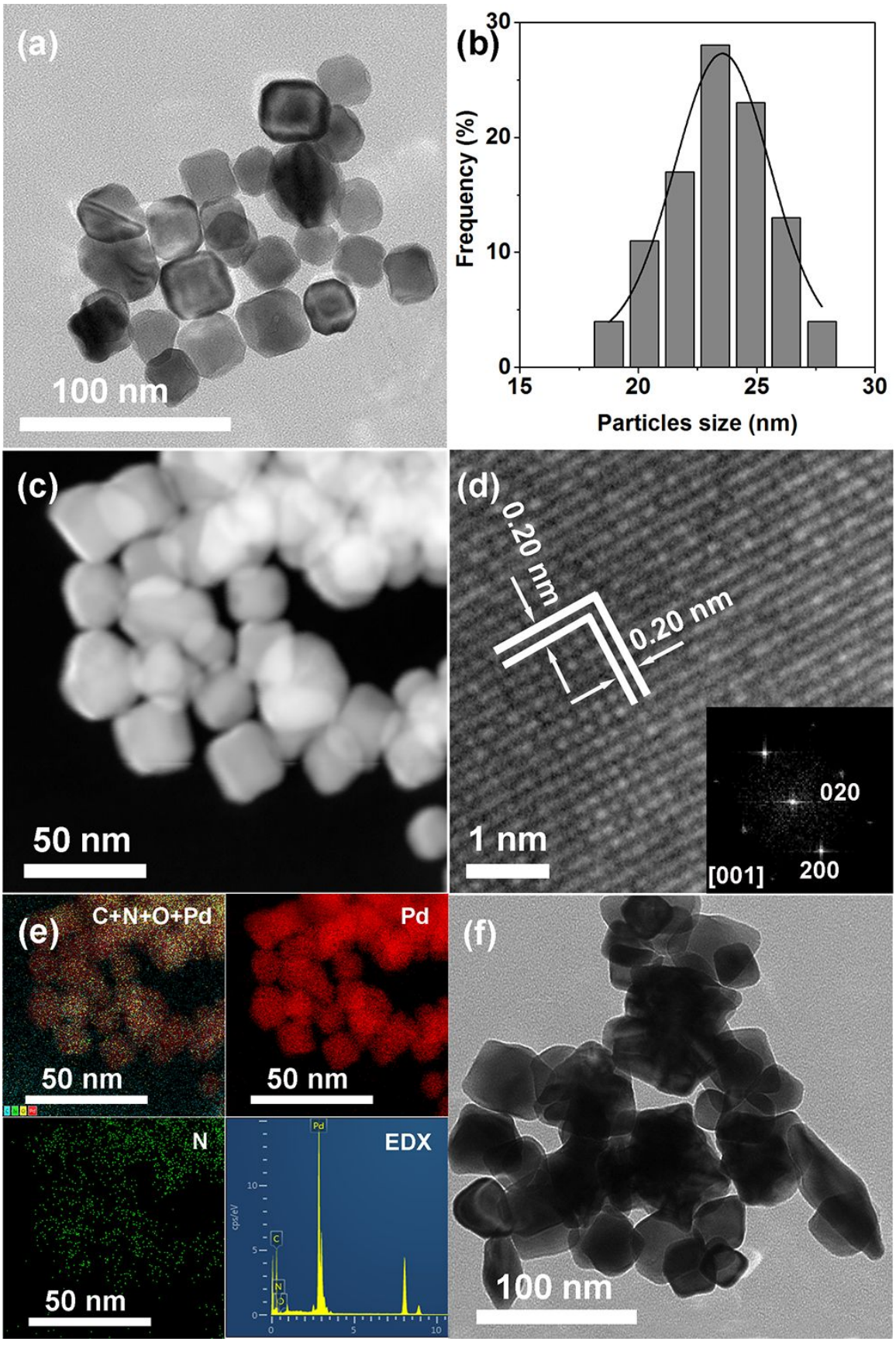
(a)
100 nm
(b)
Frequency (%)
Particles size (nm)
(c)
50 nm
(d)
0.20 nm
0.20 nm
1 nm
020
[001]
200
(e)
C+N+O+Pd
50 nm
Pd
50 nm
N
50 nm
EDX
(f)
100 nm

Figure 5. (a) TEM, (b) histograms of particle size distribution, (c) STEM, (d) HRTEM and (e) elemental mapping results of the Pd-cube-proline catalyst. Inset in (d) shows the Fourier diffractogram. (f) TEM image of Pd nanocrystals synthesized without adding S-proline.

Figure 5 shows the TEM, HRTEM and STEM results of the Pd-cube-proline catalyst. As shown in Figure 5a-5c, the dominant products are cubic nanocrystals and the average size is ~24 nm. The HRTEM image of a nanocube lying flat on the grid is shown in Figure 5d. Two dimensionally perpendicular lattice fringes are clearly observed. The d-spacing (0.20 nm) corresponds to {200} planes of fcc Pd. The Fourier diffractogram (inset in Figure 5d) exhibits regular square diffraction spot array, further confirming the enclosing of the Pd nanocubes with {100} facets and the zone axis is [001]. EDX-mapping results (Figure 5e) reveal that the atomic ratio of N/Pd is ca. 0.015 in the Pd-cube-proline sample. The amount of S-proline adsorbed on Pd-cube-proline sample is calculated to be ca. 0.06 mg, which is ca. 1.5 wt % of the Pd catalyst. Only a very small proportion (~0.005%) of S-proline added in the synthetic procedure can adsorb on the Pd-cube-proline catalyst. This fact indicates that it is unlikely to significantly increase the amount of S-proline adsorbed on the catalyst by simply increasing the quantity of S-proline added in the synthesis. How to modify the preparation procedure to dramatically increase the amount of S-proline adsorbed on the Pd nanocrystals still requires further study.

A comparison experiment was also performed under similar synthetic conditions without adding S-proline in the synthetic system. As Figure 5f shows, without S-proline, Pd nanocrystals with mixed morphologies and variable sizes were formed and tended to aggregate together. This demonstrates that the formation of {100} facets in the Pd-cube-proline catalyst is correlated with S-proline.

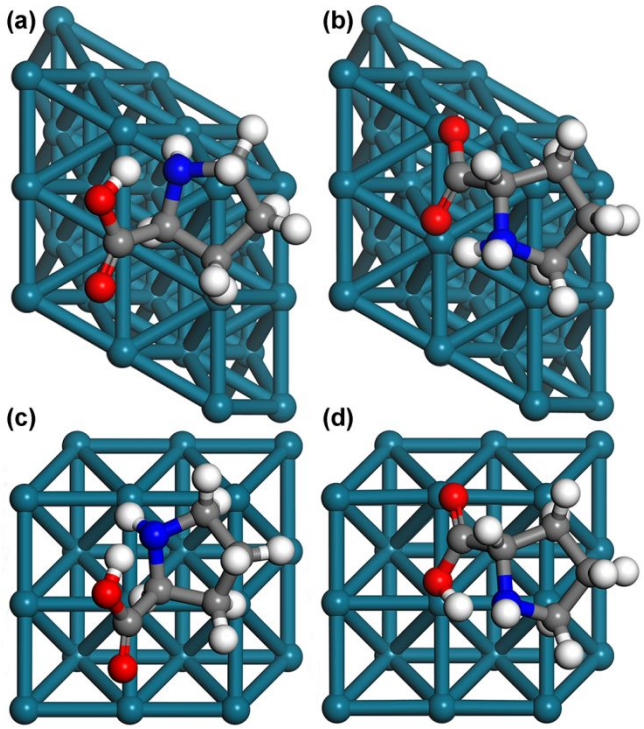

Figure 6. Adsorption of S-proline on (a, b) Pd(111) and (c, d) Pd(100) surface. (a, c) is the hydrogen-adsorption geometry and (b, d) is the oxygen-adsorption geometry.

For better understanding why S-proline can stabilize the {100} facets of fcc Pd, the adsorption of S-proline on the Pd(100) and Pd(111) surfaces was simulated using the DFT methods. S-proline is an amino acid molecule and either carboxylic group or pyrrolidine ring in S-proline has the possibility to bind to the surface Pd atoms. XPS study revealed that S-proline adsorbed on Pd(111) as a zwitterion[48]. Thus, the adsorption through the nitrogen atom from pyrrolidine is excluded. Then, only two most likely adsorption structures of S-proline were optimized. The first starting geometry is the hydrogen-adsorption from pyrrolidine ring. The second one is the oxygen-adsorption from carboxylate group. Figure 6 shows the optimized geometries. The adsorption energies (E_{ads}) for the hydrogen-adsorption geometry are -10.4 and -13.1 kcal mol^{-1} on the Pd(111) and Pd(100) surfaces, respectively. As for the oxygen-adsorption geometry, the adsorption energies are -14.1 and -16.7 kcal mol^{-1} on the Pd(111) and Pd(100) surfaces,

respectively. Obviously, the adsorption energy of S-proline on Pd(100) surface is much lower than that on Pd(111) surface for both hydrogen- and oxygen-adsorption geometry, indicating that S-proline adsorbs stronger on Pd(100) surface. Thus, S-proline probably prefers to stabilize {100} facets than {111} facets in our synthetic process, leading to the production of Pd nanocubes.

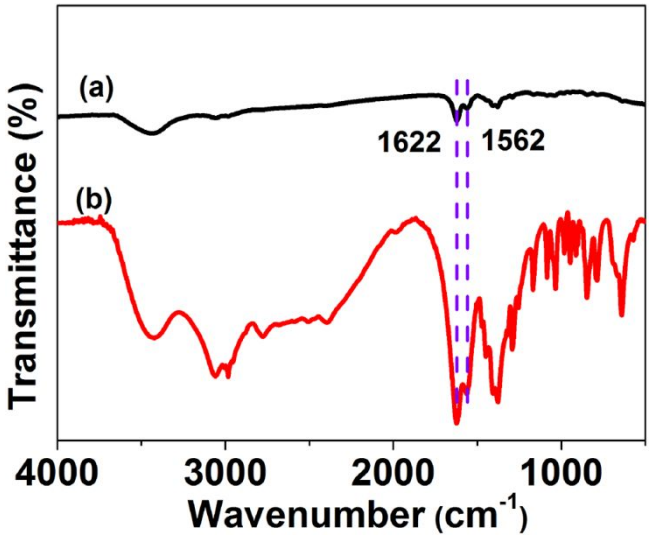

Figure 7. FT-IR spectra of Pd-cube-proline (a) and S-proline (b).

FT-IR spectra of Pd-cube-proline and pure S-proline are shown in Figure 7. The vibration bands at 1622 and 1562 cm^{-1} in the Pd-cube-proline catalyst correspond to COO^- asymmetric stretch vibrational mode and scissor bending vibration of NH_2^+ in S-proline, respectively.[49] The similar FT-IR spectra between Pd-cube-proline catalyst and pure S-proline indicate that there is S-proline binded to the surface of Pd-cube-proline catalyst.

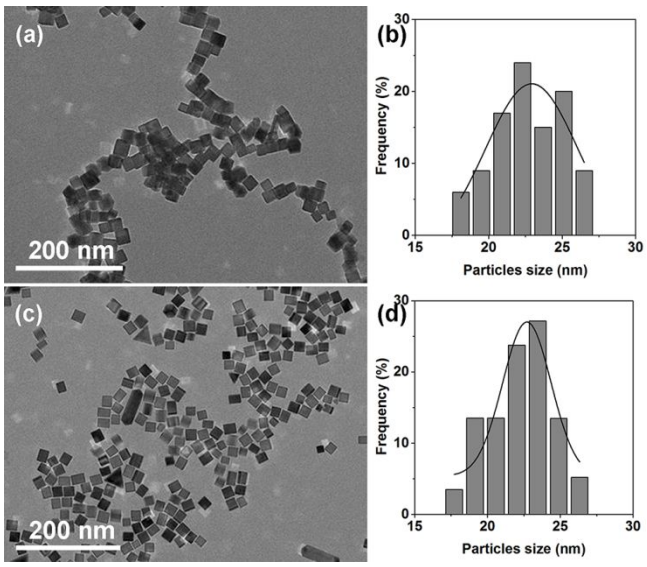

Figure 8. TEM images (a, c) and particle size distribution (b, d) of Pd-cube-CTAB (a, b) and Pd-cube-PVP (c, d).

For comparison, we also synthesized Pd nanocubes with similar particle size by using CTAB or PVP as the capping agents. Figure 8 shows the typical TEM images and histograms of particle size distribution. All the nanocube samples have similar average particle size of ~23 nm.

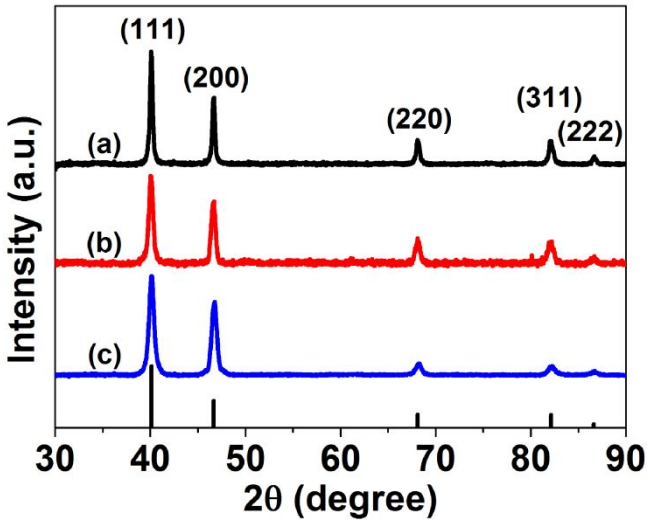

Figure 9. XRD patterns of Pd-cube-proline (a), Pd-cube-CTAB (b), Pd-cube-PVP (c) catalysts. Vertical lines represent fcc Pd (JCPDS 89-4897).

The XRD patterns of the Pd-cube-proline, Pd-cube-CTAB, and Pd-cube-PVP samples are shown in Figure 9. In all Pd nanocube samples, there are five diffraction peaks which are ascribable to reflections of fcc Pd. The Pd-cube-proline, Pd-cube-CTAB, and Pd-cube-PVP samples exhibit lattice parameter identical to that of fcc Pd (0.389 nm). The ratio of the (200) to (111) reflections in all Pd nanocube samples is similar and ~1.4 times that of JCPDS (0.60 versus 0.44). As the Pd nanocubes are prone to lying flat on the XRD sample holder, its (200) preferred orientation indicates that the nanocubes are bounded by {100} facets, consistent with the TEM results.

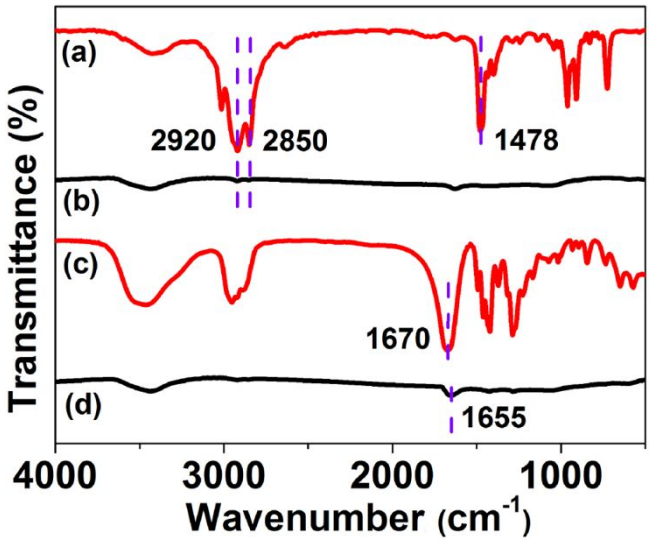

Figure 10. FT-IR spectra of CTAB (a), Pd-cube-CTAB (b), PVP (c) and Pd-cube-PVP (d).

The infrared spectrum of CTAB (Figure 10a) shows three strong vibrational bands at 1478, 2850 and 2920 cm^{-1}, corresponding to C-H scissoring vibrational mode of -N-CH_3 moiety in the CTAB, symmetric and asymmetric -CH_2 stretch vibrational mode of the CTAB, respectively.[50-51] As for the Pd-cube-CTAB sample (Figure 10b), we can still observe the two characteristic vibrations at 2920 and 2850 cm^{-1}, suggesting that CTAB is retained on the Pd nanocubes. As for pure PVP (Figure 10c), it gives the characteristic C=O stretching vibrational band at 1670 cm-

[1].[52-54] Other characteristic bands, including the C-N stretching vibrational band of N-C=O (1494 cm^{-1}), C-H scissoring vibrational mode (1424 cm^{-1}), C-H bending vibrational band (1373 cm^{-1}), and C-N stretching vibrational mode of N-CH_2 (1288 cm^{-1}), are also observed.[52-54] In the Pd-cube-PVP sample (Figure 10d), although the relative intensity of the vibrational modes ranging from 1500 to 1300 cm^{-1} decreases dramatically, the stretching vibration of C=O (1655 cm^{-1}) can still be clearly observed. The red shift and weakening of C=O stretching vibrational mode is probably related to the chemisorption of PVP on Pd surface.[54] FT-IR result suggests that PVP is retained on the surface of Pd cubic nanocrystals. Washing and centrifugation cannot totally clear the PVP bonded on the nanocubes.

3.2.2 Enantioselective hydrogenation of acetophenone

As for the S-proline modified Pd catalyst, the literature results[5] verify that it can work as an enantioselective catalyst for heterogeneous asymmetric hydrogenation of acetophenone. Thus, we tested the properties of Pd-cube-proline, Pd-cube-CTAB, and Pd-cube-PVP catalysts utilizing the acetophenone hydrogenation reaction as a probe.

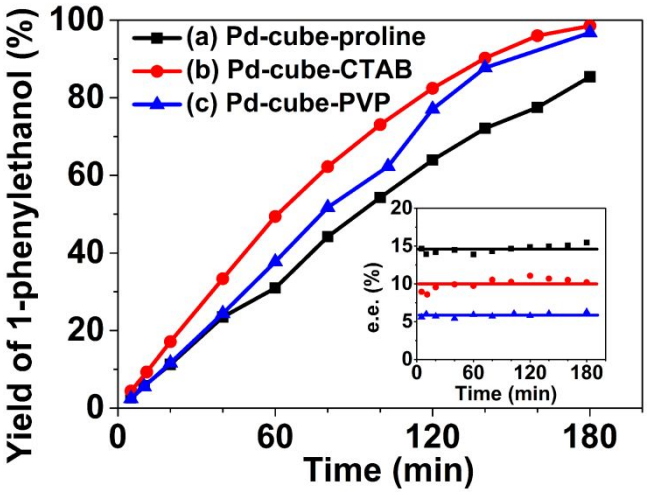

Figure 11. The enantioselective behaviors of (a) Pd-cube-proline, (b) Pd-cube-CTAB, and (c) Pd-cube-PVP catalysts. Reaction conditions: 17 mL methanol, 273 K, 20 μL acetophenone, 4 mg catalyst, 0.40 g S-proline, H_2 (60 mL min^{-1}).

Without the introduction of additional S-proline in the reaction mixture, no enantioselectivity was observed over all three nanocube catalysts. The reason of no enantioselectivity over the as-prepared Pd-cube-proline catalyst is probably due to that the amount of S-proline adsorbed on the catalyst is relatively small and not sufficient to induce chirality in the asymmetric hydrogenation of acetophenone.

Table 2. The catalytic performance of Pd-cube-proline catalyst in asymmetric hydrogenation of acetophenone after three successive runs.

Run	Yield (%)	ee (%)	Dominant Enantiomer
1	30.9	15	R
2	28.3	15	R
3	26.2	15	R

Reaction conditions: 17 mL methanol, 273 K, 20 μL acetophenone, 4 mg catalyst, 0.40 g S-proline, H_2 (60 mL min^{-1}), reaction time 1 h.

With the introduction of additional S-proline in the hydrogenation reaction mixture, as shown in Figure 11, the activity sequence of the three nanocube catalysts is Pd-cube-CTAB > Pd-cube-PVP > Pd-cube-proline. The Pd-cube-proline catalyst exhibits an average enantioselectivity of 15% with the dominant R-enantiomer, which is 1.5 times that of Pd-cube-CTAB catalyst (10%) and 2.5 times that of Pd-cube-PVP catalyst (6%). The ee sequence reveals that the adverse effect of residual CTAB on the enantioselectivity is smaller than that of PVP in acetophenone hydrogenation. Table 2 shows the catalytic performance of the Pd-cube-proline catalyst after 1

h's reaction for three successive runs. The invariable ee for three consecutive runs demonstrates that the Pd-cube-proline catalyst is highly stable, although a decrease in activity is observed. The decrease of activity after recycling is probably related to the fact that Pd nanocubes tend to aggregate in the recycled Pd-cube-proline catalyst, which is verified by TEM images of the recycled catalysts. The accumulation of S-proline adsorbed on the recycled catalyst during recovery may also lead to the decrease of activity. Despite the relative low enantioselectivity on the in-situ synthesized Pd-cube-proline catalyst, our work demonstrates that in-situ chirally modified Pd catalyst is more favorable to achieve higher enantioselectivity than CTAB or PVP-capped Pd catalysts.

With respect to acetophenone asymmetric hydrogenation, the enantioselectivities reported so far over supported Pd and Pt catalysts are generally low.[5-6, 55-56] The best result was reported by Tungler et al. over S-proline modified 10% Pd/C (Dutral), which gave 22.5% ee at 77.9% conversion.[5] However, they also found that the origin of the commercial Pd/C catalysts strongly affected the ee, which was generally below 16.7% and could be as low as 7.9%.[5] Previously, we found that by altering the confinement effect, the enantioselectivity in acetophenone hydrogenation on free-standing mesoporous Pd catalysts could be effectively tuned from 22% to 42% and the mesoporous Pd catalyst with higher (111) preferred orientation exhibited increased enantioselectivity.[57] Thus, the low enantioselectivity of the present Pd-cube-proline catalyst may derive from the fact that the Pd-cube-proline catalyst has large Pd particle size (small surface area) and exposes {100} facets. If someone could prepare in-situ chirally modified Pd nanocrystal catalyst with smaller particle size and with other specific facets, higher enantioselectivity is expected.

4. CONCLUSION

In summary, in-situ chirally modified palladium nanocrystals without capping agents were successfully prepared via a simple one-pot strategy by replacing the conventional capping agents with chiral modifiers such as CD and S-proline. Their applications in the asymmetric hydrogenation of C=O or C=C bond were studied. In the enantioselective hydrogenation of (E)-α-phenylcinnamic acid, the as-prepared CD-modified Pd nanodendrite catalyst does not require follow-up chiral modification process and shows enantioselectivity, indicating that the CD remained on the as-prepared dendritic Pd nanocrystals is already sufficient to induce chiral recognition. In the asymmetric hydrogenation of acetophenone, the as-prepared S-proline-modified Pd nanocube catalyst shows higher enantioselectivity than nanocubes synthesized with PVP or CTAB as capping agents. The direct synthesis of in-situ chirally modified palladium nanocrystals with controllable shapes by using chiral modifiers as shape-control agents offers a simple and effective method to prepare enantioselective metal nanocrystal catalysts, which may be promising in heterogeneous asymmetric catalytic reactions.

AUTHOR INFORMATION

Corresponding Author

*E-mail: xueyingchen@fudan.edu.cn

Author Contributions

The manuscript was written through contributions of all authors. All authors have given approval to the final version of the manuscript.

ACKNOWLEDGMENT

This work was supported by the National Natural Science Foundation of China (21573045, 21773034).

REFERENCES

(1) Blaser, H. U.; Pugin, B. In *Chiral Reactions in Heterogeneous Catalysis;* Jannes, G., Dubois, V., Eds.; Plenum Press: New York, 1995; pp 5-20.

(2) Klabunovskii, E.; Smith, G. V.; Zsigmond, Á. *Heterogeneous Enantioselective Hydrogenations-Theory and Practice;* Springer: Dordrecht, 2006; Vol. 31, pp 161-170.

(3) Baiker, A. Crucial Aspects in the Design of Chirally Modified Noble Metal Catalysts for Asymmetric Hydrogenation of Activated Ketones. *Chem. Soc. Rev.* **2015,** 44, 7449-7464.

(4) Meemken, F.; Baiker, A. Recent Progress in Heterogeneous Asymmetric Hydrogenation of C=O and C=C Bonds on Supported Noble Metal Catalysts. *Chem. Rev.* **2017,** 117, 11522-11569.

(5) Tungler, A.; Tarnai, T.; Mathe, T.; Petro, J. Enantioselective Hydrogenation of Acetophenone in the Presence of S-proline. *J. Mol. Catal.* **1991,** 67, 277-282.

(6) Hess, R.; Vargas, A.; Mallat, T.; Bürgi, T.; Baiker, A. Inversion of Enantioselectivity in the Platinum-catalyzed Hydrogenation of Substituted Acetophenones. *J. Catal.* **2004,** 222, 117-128.

(7) Guan, Z. H.; Lu, S. M.; Li, C. Enantioselective Hydrogenation of α,β-unsaturated Carboxylic Acid over Cinchonidine-modified Pd Nanoparticles Confined in Carbon Nanotubes. *J. Catal.* **2014,** 311, 1-5.

(8) Bui Trung, T. S.; Kim, Y.; Kang, S.; Lee, H.; Kim, S. The Enantioselective Hydrogenation of (E)-α-phenylcinnamic Acid: Role of TiO_2 Coated on Al_2O_3 as a Novel Support for Cinchonidine-modified Pd Catalysts. *Catal. Commun.* **2015,** 66, 21-24.

(9) Li, C. Chiral Synthesis on Catalysts Immobilized in Microporous and Mesoporous Materials. *Catal. Rev. - Sci. Eng.* **2004,** 46, 419-492.

(10) Hoxha, F.; Schimmoeller, B.; Cakl, Z.; Urakawa, A.; Mallat, T.; Pratsinis, S. E.; Baiker, A. Influence of Support Acid–base Properties on the Platinum-catalyzed Enantioselective Hydrogenation of Activated Ketones. *J. Catal.* **2010,** 271, 115-124.

(11) Davis, M. E.; Davis, R. J. *Fundamentals of Chemical Reaction Engineering;* McGraw-Hill Higher Education: New York, 2003; pp 149-153.

(12) Burda, C.; Chen, X. B.; Narayanan, R.; El-Sayed, M. A. Chemistry and Properties of Nanocrystals of Different Shapes. *Chem. Rev.* **2005,** 105, 1025-1102.

(13) Zhang, Y.; Wang, M. S.; Zhu, E. B.; Zheng, Y. B.; Huang, Y.; Huang, X. Q. Seedless Growth of Palladium Nanocrystals with Tunable Structures: From Tetrahedra to Nanosheets. *Nano Lett.* **2015,** 15, 7519-7525.

(14) Zhao, X. J.; Zhao, Y.; Fu, G.; Zheng, N. F. Origin of the Facet Dependence in the Hydrogenation Catalysis of Olefins: Experiment and Theory. *Chem. Commun.* **2015,** 51, 12016-12019.

(15) Schmidt, E.; Vargas, A.; Mallat, T.; Baiker, A. Shape-selective Enantioselective Hydrogenation on Pt Nanoparticles. *J. Am. Chem. Soc.* **2009,** 131, 12358-12367.

(16) Zhang, H.; Jin, M. S.; Xiong, Y. J.; Lim, B.; Xia, Y. N. Shape-controlled Synthesis of Pd Nanocrystals and Their Catalytic Applications. *Acc. Chem. Res.* **2013,** 46, 1783-1794.

(17) Ruditskiy, A.; Peng, H.-C.; Xia, Y. N. Shape-controlled Metal Nanocrystals for Heterogeneous Catalysis. *Annu. Rev. Chem. Biomol. Eng.* **2016,** 7, 327-348.

(18) Wu, B. H.; Zheng, N. F. Surface and Interface Control of Noble Metal Nanocrystals for Catalytic and Electrocatalytic Applications. *Nano Today* **2013,** 8, 168-197.
(19) Koczkur, K. M.; Mourdikoudis, S.; Polavarapu, L.; Skrabalak, S. E. Polyvinylpyrrolidone (PVP) in Nanoparticle Synthesis. *Dalton. Trans.* **2015,** 44, 17883-17905.
(20) Lopez-Sanchez, J. A.; Dimitratos, N.; Hammond, C.; Brett, G. L.; Kesavan, L.; White, S.; Miedziak, P.; Tiruvalam, R.; Jenkins, R. L.; Carley, A. F.; Knight, D.; Kiely, C. J.; Hutchings, G. J. Facile Removal of Stabilizer-ligands from Supported Gold Nanoparticles. *Nat. Chem.* **2011,** 3, 551-556.
(21) Crespo-Quesada, M.; Andanson, J. M.; Yarulin, A.; Lim, B.; Xia, Y. N.; Kiwi-Minsker, L. UV-ozone Cleaning of Supported Poly(vinylpyrrolidone)-stabilized Palladium Nanocubes: Effect of Stabilizer Removal on Morphology and Catalytic Behavior. *Langmuir* **2011,** 27, 7909-7916.
(22) Li, D. G.; Wang, C.; Tripkovic, D.; Sun, S. H.; Markovic, N. M.; Stamenkovic, V. R. Surfactant Removal for Colloidal Nanoparticles from Solution Synthesis: The Effect on Catalytic Performance. *ACS Catal.* **2012,** 2, 1358-1362.
(23) Niu, Z. Q.; Li, Y. D. Removal and Utilization of Capping Agents in Nanocatalysis. *Chem. Mater.* **2014,** 26, 72-83.
(24) Luo, M. H.; Hong, Y. C.; Yao, W. F.; Huang, C. P.; Xu, Q. J.; Wu, Q. Facile Removal of Polyvinylpyrrolidone (PVP) Adsorbates from Pt Alloy Nanoparticles. *J. Mater. Chem. A* **2015,** 3, 2770-2775.
(25) Su, N.; Gao, X. Y.; Chen, X. Y.; Yue, B.; He, H. Y. The Enantioselective Hydrogenation of Acetophenone over Pd Concave Tetrahedron Nanocrystals Affected by the Residual Adsorbed Capping Agent Polyvinylpyrrolidone (PVP). *J. Catal.* **2018,** 367, 244-251.
(26) Bönnemann, H.; Braun, G. A. Enantioselective Hydrogenations on Platinum Colloids. *Angew. Chem. Int. Ed.* **1996,** 35, 1992-1995.
(27) Bönnemann, H.; Braun, G. A. Enantioselectivity Control with Metal Colloids as Catalysts. *Chem. Eur. J.* **1997,** 3, 1200-1202.
(28) Rodrigues, T. S.; Zhao, M.; Yang, T.-H.; Gilroy, K. D.; da Silva, A. G. M.; Camargo, P. H. C.; Xia, Y. Synthesis of Colloidal Metal Nanocrystals: A Comprehensive Review on the Reductants. *Chem. Eur. J.* **2018,** 24, 16944-16963.
(29) Niu, W. X.; Zhang, L.; Xu, G. B. Shape-controlled Synthesis of Single-crystalline Palladium Nanocrystals. *ACS Nano* **2010,** 4, 1987-1996.
(30) Jin, M. S.; Liu, H. Y.; Zhang, H.; Xie, Z. X.; Liu, J. Y.; Xia, Y. N. Synthesis of Pd Nanocrystals Enclosed by {100} Facets and with Sizes <10 nm for Application in CO Oxidation. *Nano Res.* **2010,** 4, 83-91.
(31) Junquera, J.; Paz, O.; Sanchez-Portal, D.; Artacho, E. Numerical Atomic Orbitals for Linear-scaling Calculations. *Phys. Rev. B* **2001,** 64, 235111.
(32) Troullier, N.; Martins, J. L. Efficient Pseudopotentials for Plane-wave Calcualations. *Phys. Rev. B* **1991,** 43, 1993-2006.
(33) Perdew, J. P.; Burke, K.; Ernzerhof, M. Generalized Gradient Approximation Made Simple. *Phys. Rev. Lett.* **1996,** 77, 3865-3868.
(34) ScaLAPACK Home Page. http://www.netlib.org/scalapack/scalapack_home.html (accessed Aug 17, 2018).
(35) Eichler, A.; Mittendorfer, F.; Hafner, J. Precursor-mediated Adsorption of Oxygen on the (111) Surfaces of Platinum-group Metals. *Phys. Rev. B* **2000,** 62, 4744-4755.
(36) Nitta, Y. Importance of Product Desorption in Enantioselective Hydrogenation of (E)-α-

phenylcinnamic Acid with a Cinchonidine-modified Pd/TiO_2 Catalyst: Effect of Additives. *Chem. Lett.* **1999**, 635-636.

(37) Meemken, F.; Maeda, N.; Hungerbühler, K.; Baiker, A. Heterogeneous Asymmetric Hydrogenation of Prochiral Alkenoic Acid: Origin of Rate and Enantioselectivity Enhancement by Amine Addition. *ACS Catal.* **2012,** 2, 464-467.

(38) Huang, X. Q.; Tang, S. H.; Mu, X. L.; Dai, Y.; Chen, G. X.; Zhou, Z. Y.; Ruan, F. X.; Yang, Z. L.; Zheng, N. F. Freestanding Palladium Nanosheets with Plasmonic and Catalytic Properties. *Nat. Nanotechnol.* **2011,** 6, 28-32.

(39) Lim, B.; Jiang, M. J.; Yu, T.; Camargo, P. H. C.; Xia, Y. N. Nucleation and Growth Mechanisms for Pd-Pt Bimetallic Nanodendrites and Their Electrocatalytic Properties. *Nano Res.* **2010,** 3, 69-80.

(40) Lim, B.; Xia, Y. N. Metal Nanocrystals with Highly Branched Morphologies. *Angew. Chem. Int. Ed.* **2011,** 50, 76-85.

(41) Watt, J.; Cheong, S.; Tilley, R. D. How to Control the Shape of Metal Nanostructures in Organic Solution Phase Synthesis for Plasmonics and Catalysis. *Nano Today* **2013,** 8, 198-215.

(42) Ferri, D.; Burgi, T. An in situ Attenuated Total Reflection Infrared Study of a Chiral Catalytic Solid-liquid Interface: Cinchonidine Adsorption on Pt. *J. Am. Chem. Soc.* **2001,** 123, 12074-12084.

(43) Ferri, D.; Burgi, T.; Baiker, A. In situ ATR-IR Study of the Adsorption of Cinchonidine on Pd/Al_2O_3: Differences and Similarities with Adsorption on Pt/Al_2O_3. *J. Catal.* **2002,** 210, 160-170.

(44) Behzadi, B.; Vargas, A.; Ferri, D.; Ernst, K.-H.; Baiker, A. Cinchonidine Adsorption on Gold and Gold-containing Bimetallic Platinum Metal Surfaces: An Attenuated Total Reflection Infrared and Density Functional Theory Study. *J. Phys. Chem. B* **2006,** 110, 17082-17089.

(45) Reschetilowski, W.; Böhmer, U.; Wiehl, J. Pt-containing Zeolites for Enantioselective Catalytic Hydrogenation of Ethylpyruvate – Effects of Zeolite Structures, Solvent and Modifier Concentration. *Stud. Surf. Sci. Catal.* **1994,** 84, 2021-2028.

(46) Nitta, Y.; Kobiro, K.; Okamoto, Y. Enantioselective Hydrogenation of (E)-α-phenylcinnamic Acid on Cinchonidine-modified Palladium Catalysts: Influence of Support. *Stud. Surf. Sci. Catal.* **1997,** 108, 191-198.

(47) Kubota, T.; Kubota, H.; Kubota, T.; Moriyasu, E.; Uchida, T.; Nitta, Y.; Sugimura, T.; Okamoto, Y. Enantioselective Hydrogenation of (E)-α-phenylcinnamic Acid over Cinchonidine-modified Pd Catalysts Supported on TiO_2 and CeO_2. *Catal. Lett.* **2009,** 129, 387-393.

(48) Gao, F.; Wang, Y. L.; Burkholder, L.; Tysoe, W. T. Chemistry of L-proline on Pd(111): Temperature-programmed Desorption and X-ray Photoelectron Spectroscopic Study. *Surf. Sci.* **2007,** 601, 3579-3588.

(49) Herlinger, A. W.; Long, T. V. Laser-Raman and Infrared Spectra of Amino Acids and Their Metal Complexes. III. Proline and Bisprolinato Complexes. *J. Am. Chem. Soc.* **1970,** 92, 6481-6486.

(50) Wang, Y.; Chen, X. Y.; Yue, B.; He, H. Y. Self-assembly of Mesoporous Ni–P Nanosphere Catalyst with Uniform Size and Enhanced Catalytic Activity in Nitrobenzene Hydrogenation. *Top. Catal.* **2012,** 55, 1022-1031.

(51) Mehta, S. K.; Kumar, S.; Chaudhary, S.; Bhasin, K. K.; Gradzielski, M. Evolution of ZnS Nanoparticles via Facile CTAB Aqueous Micellar Solution Route: A Study on Controlling Parameters. *Nanoscale Res. Lett.* **2009,** 4, 17-28.

(52) Borodko, Y.; Habas, S. E.; Koebel, M.; Yang, P.; Frei, H.; Somorjai, G. A. Probing the

Interaction of Poly(vinylpyrrolidone) with Platinum Nanocrystals by UV-Raman and FTIR. *J. Phys. Chem. B* **2006,** 110, 23052-23059.

(53) Oh, T.-J.; Nam, J.-H.; Jung, Y. M. Molecular Miscible Blend of Poly(2-cyano-1,4-phenyleneterephthalamide) and Polyvinylpyrrolidone Characterized by Two-dimensional Correlation FTIR and Solid State ^{13}C NMR Spectroscopy. *Vib. Spectrosc.* **2009,** 51, 15-21.

(54) Xian, J. Y.; Hua, Q.; Jiang, Z. Q.; Ma, Y. S.; Huang, W. X. Size-dependent Interaction of the Poly(N-vinyl-2-pyrrolidone) Capping Ligand with Pd Nanocrystals. *Langmuir* **2012,** 28, 6736-6741.

(55) Perosa, A.; Tundo, P.; Selva, M. Multiphase Heterogeneous Catalytic Enantioselective Hydrogenation of Acetophenone over Cinchona-modified Pt/C. *J. Mol. Catal. A-Chem.* **2002,** 180, 169-175.

(56) Vetere, V. New Approach Toward the Synthesis of Asymmetric Heterogeneous Catalysts for Hydrogenation Reactions. *J. Catal.* **2004,** 226, 457-461.

(57) Wang, Y.; Su, N.; Ye, L.; Ren, Y. H.; Chen, X. Y.; Du, Y.; Li, Z. H.; Yue, B.; Tsang, S. C. E.; Chen, Q.; He, H. Y. Tuning Enantioselectivity in Asymmetric Hydrogenation of Acetophenone and Its Derivatives via Confinement Effect over Free-standing Mesoporous Palladium Network Catalysts. *J. Catal.* **2014,** 313, 113-126.

Table of Contents